promoting access to White Rose research papers

Universities of Leeds, Sheffield and York
http://eprints.whiterose.ac.uk/

This is an author produced version of a paper published in **The Journal of Chemical Physics.**

White Rose Research Online URL for this paper:
http://eprints.whiterose.ac.uk/7972/

Published paper

Vondrak, T., Meech, S.R. and Plane, J.M.C. (2009) *Photoelectric emission from the alkali metal doped vacuum-ice interface.* The Journal of Chemical Physics, 130 (5). 054702.
http://dx.doi.org/10.1063/1.3063658

White Rose Research Online
eprints@whiterose.ac.uk

THE JOURNAL OF CHEMICAL PHYSICS **130**, 1 (2009)

Photoelectric emission from the alkali metal doped vacuum-ice interface

Tomas Vondrak,[1] Stephen R. Meech,[2,a)] and John M. C. Plane[1,a)]
[1]*School of Chemistry, University of Leeds, Leeds LS2 9JT, United Kingdom*
[2]*School of Chemical Sciences and Pharmacy, University of East Anglia, Norwich NR4 7TJ, United Kingdom*

(Received 16 September 2008; accepted 12 December 2008; published online xx xx xxxx)

The photoelectron photoemission spectra and thresholds for low coverages of Li and K adsorbed on water-ice have been measured, compared with photoionization spectra of the gas-phase atoms, and modeled by quantum chemical calculations. For both alkali metals the threshold for photoemission is dramatically decreased and the cross section increased on adsorption to the water-ice surface. Quantum chemical calculations suggest that the initial state is formed by the metal atoms adsorbed into the water-ice surface, forming a state with a delocalized electron distribution. This state is metastable and decays on the hundreds of seconds time scale at 92 K. The decay is markedly faster for Li than for K, probably due to diffusion into the ice film. © *2009 American Institute of Physics*. [DOI: 10.1063/1.3063658]

I. INTRODUCTION

Photon and electron driven chemistry in water-ice or at the water-ice interface is believed to be significant in the chemistry and physics of both terrestrial and planetary atmospheres. Examples include formation of molecular oxygen and other products during high energy (>10 eV) photolysis,[1] hydrogen ion desorption and oxygen generation under electron bombardment,[2] electron and photon-induced chemistry of adsorbates on water-ice,[3,4] and the charging of nanosized ice particles in the mesosphere, leading to reduced mobility of the plasma around the particles and hence to the strong radar backscatter known as polar mesospheric summer echoes.[5,6]

The structure, dynamics, and chemistry of electrons solvated in or at the surface of water-ice have attracted particular attention. The ultrafast dynamics of electrons photoinjected into thin water-ice films on metal substrates were studied in detail by Bovensiepen and co-workers.[7–9] They found that electron transfer from the optically excited substrate into the ice conduction band was followed by solvation leading to electron localization on an ultrafast time scale. The solvated electrons were reported to have picosecond lifetimes, mainly limited by tunneling back to the metal substrate. Significantly, the electron lifetime was found to be morphology dependent, with evidence that the electron was localized at the ice-vacuum interface for water-ice clusters on metal substrates.[9] Sanche and co-workers studied the effect of electron attachment to water-ice films following low-energy electron bombardment.[3,10,11] They found that the solvated electrons formed following attachment from the gas phase have relatively long lifetimes, and support a variety of chemical reactions, including dissociative electron attachment to halocarbons. These authors proposed that such electron induced chemistry could be important in the reactions underlying ozone depletion in the stratosphere above the Arctic and Antarctic.[11]

Previously we investigated photoemission from ice films which had been doped with low coverages (<0.02 ML) of sodium atoms.[12,13] The motivation for those studies was also the understanding of atmospheric phenomena, specifically the reported coexistence of the positively charged particles with an excess electron population in polar mesospheric clouds.[6,14] It was found that photoemission from the Na doped water-ice surface had a surprisingly large cross section ($>10^{-18}$ cm^2 per Na atom) in the visible region of the spectrum with a threshold near 2.3 eV.[12,13] This is considerably below the 8.7 eV threshold for the ionization of undoped water-ice.[15] These photoemission studies were complemented both by measurements of the transmission spectrum and by density functional theory (DFT) calculations of the Na doped water-ice surface. The initial state for photoemission was found to be a metastable surface trapped electron associated with Na atoms accommodated in the first layer of the ice surface.[12,13] Gunster *et al.*[16] also studied Na adsorbed on water-ice using metastable electron impact spectroscopy. They observed that at 100 K a reorganization of the ice was required for solvation of the 3*s* Na atom, and that this process was temperature dependent.

In this paper, we extend both photoemission measurements and DFT calculations to the cases of lithium and potassium doped water-ice surfaces. Both alkali metals make interesting contrasts with Na. In the case of Li, although the ionization potential of the atom is higher than for Na [5.39 eV compared with 5.13 eV (Ref. 17)], the atomic radius is smaller [2.05 Å compared with 2.23 Å (Ref. 17)] so that Li can potentially penetrate more readily into the ice surface where increased interaction with the lone pairs on the oxygen atoms of the water molecules should support delocalization of the outer *s* electron. In contrast, the K atom is significantly

---

[a)] Authors to whom correspondence should be addressed. Electronic addresses: j.m.c.plane@leeds.ac.uk and s.meech@uea.ac.uk.

0021-9606/2009/130(4)/1/0/$25.00

© 2009 American Institute of Physics

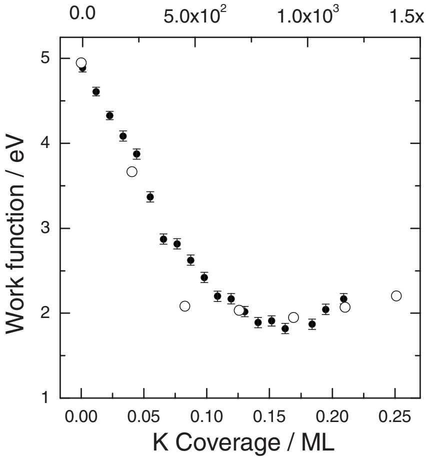

FIG. 1. Dependence of the work function of the Cu(111) surface on the K coverage. The filled points are from TPPE and the open circles are the measurement of Dudde *et al.* (Ref. 28) where coverage was established by low-energy electron diffraction and Auger electron spectroscopy.

larger than Na [2.77 Å compared with 2.23 Å (Ref. 17)], which may offset its much lower ionization potential [4.34 eV compared with 5.13 eV (Ref. 17)].

II. EXPERIMENTAL

A. Sample preparation

The method of preparation of AM doped water-ice surfaces was essentially as described previously,[13] so only the key points will be repeated here. The ultrahigh vacuum chamber consisted of an upper preparation and characterization level and a lower level housing an electron time-of-flight (eTOF) analyzer. The substrate for all experiments was a Cu(111) single crystal in thermal contact with a liquid nitrogen reservoir. The base temperature was 92 K and the substrate temperature was controlled by resistive heating. The substrate was dosed with either the AM (for calibration measurements, see below) or water. The AMs were deposited from shrouded dispensers (SEAE Getters) and water from a collimated effusive source. The rate of water deposition was calibrated from measurements of the temperature programed desorption (detected by a quadrupole mass spectrometer) as a function of dosing time. In the experiments described in Sec. III, a 3000 L (1 L$=10^{-6}$ Torr s) thick film of ice was first deposited onto the Cu(111) substrate, prior to adsorption of the AMs. Such a thick ice film ensured that the electrons detected arise only from the ice-vacuum interface and not from the metal-ice interface.

Deposition of water onto Cu(111) at 92 K yields a porous amorphous ice film.[18] These films were annealed to a temperature of 160 K prior to deposition of the AM. This was done for two reasons. First, the motivation for these experiments is the investigation of photoinduced charging phenomena in ice particles in the upper atmosphere. Annealing to 160 K, which converts the amorphous film to a cubic ice phase,[18] yields a surface more relevant to ice particles in the mesosphere.[19] Second, the amorphous ice film apparently becomes charged, which strongly perturbs the eTOF measurements.[13] The charging effect is absent in the crystalline film, suggesting that the amorphous phase is less conducting and/or has more electron binding sites than the crystalline film.[13] After annealing, the sample was returned to 92 K and the calibrated amount of the AM was deposited.

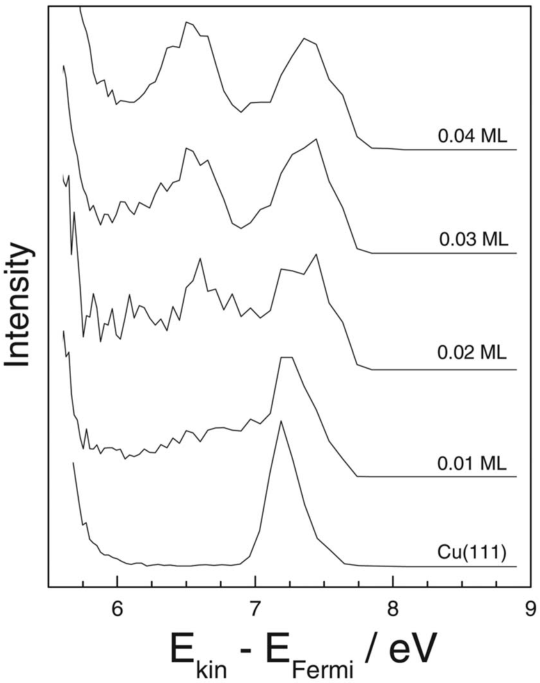

FIG. 2. The dependence of TPPE spectra of K/Cu(111) on the coverage at a photon energy of 3.8 eV. Data are plotted as photoemission intensity as a function of the final state energy.

B. Calibration

The eTOF spectrometer was calibrated from the TOF spectrum measured following the two-photon excitation of the clean well-ordered Cu(111) substrate, assuming the well-characterized surface state to be located 0.4 eV below the Fermi level (E_F),[20] a work function of 4.95 eV,[21] and utilizing the known energy of the incident photons. Radiation was from a 10 Hz, 5 ns pulse width dye laser pumped by the third harmonic of a neodymium-doped yttrium aluminum garnet laser. The laser was *p* polarized and incident on the surface at 45° to the surface normal for all measurements.

The coverage of AM was determined as follows. From the calibrated eTOF spectrum, it is straightforward to determine the work function as a function of exposure time to a fixed flux of AM. By comparing these data with literature measurements of the work function as a function of AM coverage, the exposure time required for a specific coverage of AM is obtained. Literature data are available for the coverage-dependent work function of all three AMs studied.[22] As an example, data for K on Cu(111) are shown in Fig. 1. As can be seen, the profile of the coverage-dependent work function is accurately reproduced by the exposure-dependent work function obtained from the eTOF measurements.

The two-photon photoemission (TPPE) spectra for the Cu(111)/AM surfaces as a function of photon energy ($h\nu$) and coverage are of interest in their own right.[20,22–24] The

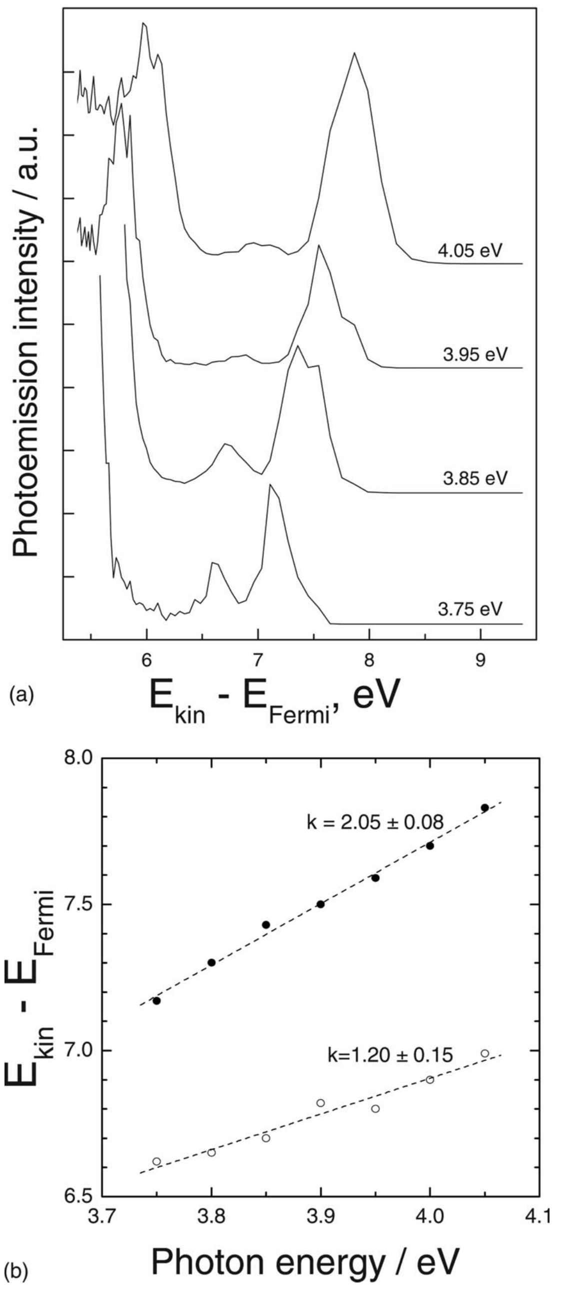

FIG. 3. (a) TPPE spectra for .05 ML Li/Cu(111) at the indicated photon energies. (b) Position of the resonance (○) and the surface state (●) from TPPE spectra for 0.05 ML Li/Cu(111). The dashed lines are least-squares linear fits.

spectra as a function of K coverage are shown in Fig. 2 and the energy dependence for the Cu(111)/0.05 L Li surface in Fig. 3. For the clean Cu(111) surface, the TPPE spectrum shows the surface state located 0.4 eV below E_F. On adsorption of low coverages of K, the surface state disappears being replaced (or obscured) by a higher energy feature plus an additional band at lower energy, which grows in with increasing K coverage. Very similar behavior was seen for Cu(111)/Na and Li surfaces, although for Li the lower energy feature is weaker [Fig. 3(a)]. The dependence of the eTOF spectrum on $h\nu$ for the Li doped surface is significant. As the incident photon energy is changed by $\Delta h\nu$, the higher energy feature shifts by 2 $\Delta h\nu$, while the lower energy one shifts by $\Delta h\nu$ [Fig. 3(b)]. Thus the higher energy feature can be assigned to an AM induced state which is occupied and lies close to E_F. The linear dependence on $h\nu$ for the lower energy feature identifies it as an unoccupied intermediate state.[25] These data are consistent with a model in which AM adsorption leads to a new occupied state close to E_F and an unoccupied state ~3 eV above E_F, shifting lower with increasing coverage. The latter can probably be assigned to an AM induced image state, as described by Fischer *et al.*[24] Very recently Zhao *et al.* reported TPPE measurements for all AMs on both Cu(111) and Ag(111).[26] They reported an image state 2 eV above E_F and characterized it in detail. The picture for the occupied state is a little less clear-cut for the K doped surface, where the energy of the TPPE signal as a function of $h\nu$ was found to have a slope of 1.3 rather than the expected value of 2. The origin of this is unknown, but the result may suggest a mixed contribution from both an occupied initial state and an unoccupied intermediate state higher in energy than the image state.

III. RESULTS AND DISCUSSION

The yield of electrons from the Cu(111) substrate is a strong function of laser intensity, reflecting the nonlinear (two-photon) origin of the signal. When the Cu(111) crystal is coated with only 4 L of water, the photoemission is strongly attenuated, consistent with trapping of electrons in the ice film and their subsequent ultrafast tunneling back to the substrate.[7,27] When the 4 L film is replaced by a 3000 L thick film and the same laser intensity is used, no photoemission is detected from the film, reflecting the high photoionization (PI) threshold for water-ice. On application of even 0.02 L of AM, the same laser intensity yields a saturating electron current. The origin of this extremely high yield of photoemission was established for Na on water-ice to be a very low threshold, so low, in fact, that single photon ionization was occurring.[12,13] This was established by a linear intensity dependence at very low fluence (0.1–1 μJ cm^{-2}).

Very similar behavior to that previously reported for Na on water-ice was found for both Li and K deposited at less than 0.05 L. The photoemission yields as a function of $h\nu$ for both AMs are shown in Fig. 4. In both cases, photoemission is detectable for photon energies as low as 2 eV, but the yield climbs more or less exponentially between 2.1 and 3.5 eV for K doped water-ice and 2.5 and 3.25 eV for the Li doped film. These data are remarkably similar to those previously observed for Na (cross section rising between 2.3 and 3.0 eV) and taken together suggest a common origin for the initial state, with a slight tendency for the threshold to decrease for the heavier AM (although the effect is not large compared with the error of ±0.2 eV in determining the threshold).

The energy distribution of the photoemitted electrons is shown for 0.02 L K on water-ice as a function of $h\nu$ in Fig. 5. For $h\nu$ at and slightly above threshold (2.2 and 2.6 eV), an asymmetric electron kinetic energy profile is observed, with the lower limit being set by the ionization threshold and the upper one by the photon energy. As $h\nu$ increases, the photons sample deeper within the band of the initial state and the

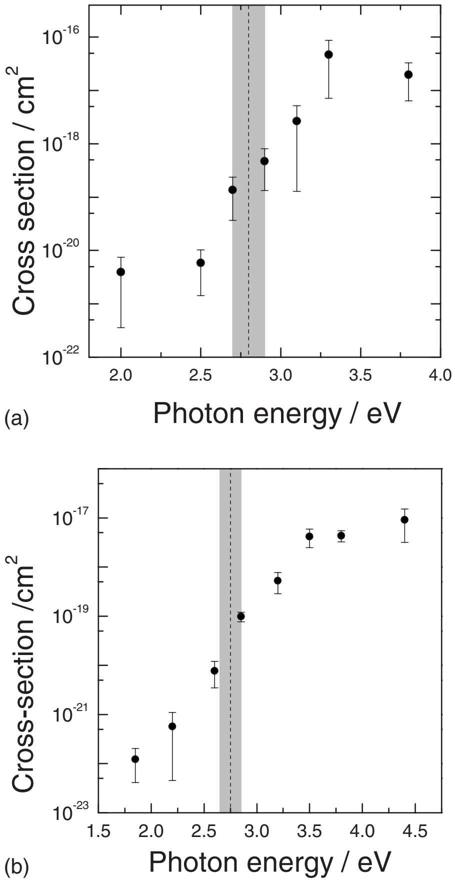

FIG. 4. Photon energy dependence of the photoemission cross section of the water-ice surface doped with (a) 0.05 ML of Li and (b) 0.02 ML of potassium. The gray line indicates the inflection point for the sigmoid shaped curve. The laser beam was *p*-polarized and incident on the film at 45°.

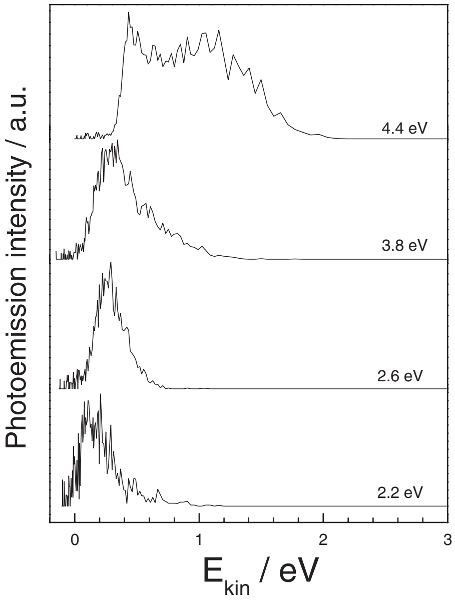

FIG. 5. Photon energy dependence of the photoelectron spectra for 0.02 ML of K on water-ice.

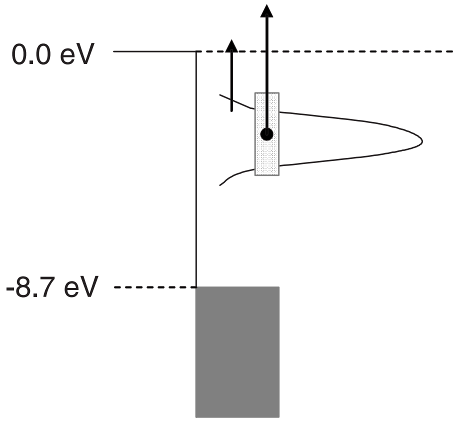

FIG. 6. Schematic indicating the origin of the energy dependent spectra shown in Fig. 5.

curve broadens until, at high photon energy, a discrete band is observed; very similar behavior was observed for Li and Na.

Thus the strong similarities between the photoemission spectra for the three AMs are also consistent with a common initial state. Taking the vacuum level as 0 eV and assuming the highest occupied level of water to be at -8.7 eV (i.e., the photoemission threshold for pure water-ice), the threshold data (Fig. 4) locate the highest energy edge of the initial state to be at -2.5 eV for Li and slightly higher for Na and K. The photoemission spectra (Fig. 5) suggest an inhomogeneous distribution of sites for the initial state, with population increasing for more negative energies. The appearance of a discrete peak in the TOF spectrum at $h\nu > 4.4$ eV indicates that the energy width of the inhomogeneous site distribution is at least 2 eV. This is illustrated in Fig. 6, where the lower energy photons sample only the high energy edge of the distributions, while increasing $h\nu$ samples deeper into (and eventually all of) the distribution, leading to broader and more intense photoemission spectra.

Figure 4 also illustrates the PI cross section spectra for Li and K on ice, calculated in the same way as previously for Na.[13] The peak absolute cross section for photoemission was measured to be $(5 \pm 2) \times 10^{-18}$ cm^2 atom^{-1} for K, $(3 \pm 2) \times 10^{-18}$ cm^2 atom^{-1} for Na,[13] and a somewhat higher value for Li of $(5 \pm 4) \times 10^{-17}$ cm^2 atom^{-1}. Figure 7 shows the PI spectra for the three alkali atoms in the gas phase.[28] The peak cross sections are 8.1×10^{-20} cm^2 atom^{-1} for K, 1.0×10^{-19} cm^2 atom^{-1} for Na, and 1.7×10^{-18} cm^2 atom^{-1} for

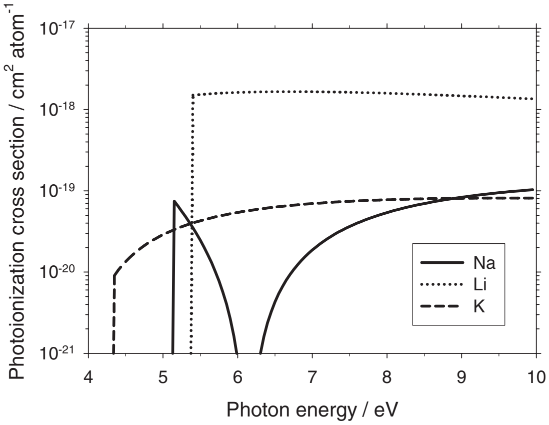

FIG. 7. PI cross sections for atomic Li, Na, and K in the gas phase, as a function of photon energy (Ref. 27).

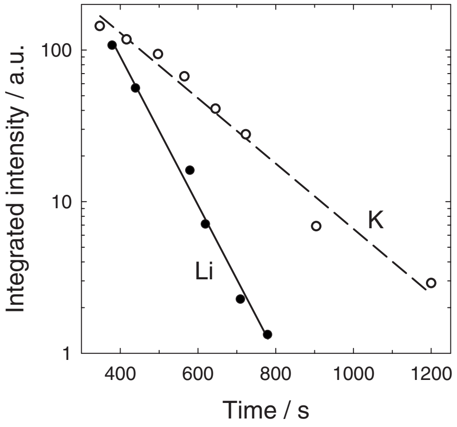

FIG. 8. Time-resolved decays of PI cross section. ○: the decay of K species formed by the deposition of 0.02 ML of K on 3000 L of H_2O. The photoemission signal was obtained with the photon energy of 4.4 eV. The decay rate is $(5\pm2)\times10^{-3}$ s^{-1} (dashed-line). ●: the decay of the low-energy feature of 0.05 ML of Li in 3000 L of H_2O. Photon energy of 3.3 eV. The average value of the decay rate obtained from 5 data sets is $(1.4\pm0.4)\times10^{-2}$ s (solid line). Measurements commenced 250 s after deposition was completed to allow the chamber to return to operating pressure and the surface to be transferred to the spectrometer.

Li. Thus the Li cross section is ~20 times larger than the cross sections of Na and K (which are approximately equal), both on the ice surface and in the gas phase. Furthermore, the cross section of each AM is ~30 times larger when the atom is adsorbed on ice, compared with the gas phase. A final point is that the PI spectrum of Na/ice decreased by two orders of magnitude for photon energies between 3.6 and 4.4 eV,[13] in contrast with the results from the present study for Li and K on ice (Fig. 4). This behavior is again consistent with the gas-phase PI spectra (Fig. 7).

The initial state when the AM adsorbs on the ice surface is suggested to be a metastable form of a solvated electron only loosely associated with its parent AM atom (see below). This assignment is based on a number of factors. First, as noted above, the PI cross sections for all three AMs in the gas phase increase approximately 30-fold when the atoms are adsorbed on ice. Second, we measured the transmission spectrum of Na adsorbed on water-ice and observed a broad band peaked around 2 eV,[12] which is strikingly similar to the spectrum of the solvated electron formed in γ-irradiated ice.[29] Finally, studies of the ionization potential of Na atom doped water clusters in the gas phase were measured as 3.2 eV which is close to the threshold values recorded here.[30]

The picture emerging of a strong similarity between the behaviors of the three AMs on the water-ice surface breaks down when we consider the lifetime of the state formed on deposition. In our study of Na on water-ice, it was observed that the initial state was metastable and disappeared with a temperature-dependent rate coefficient characterized by an activation energy of around 10 kJ mol^{-1}.[13] This decay of the initial state was assigned to more complete solvation of the Na anion in the bulk of the ice and localization of the electron to form OH^-. Measurements of the decay of the initial state formed on adsorption of the other AMs were made at 92 K (Fig. 8). A wide range in the first-order rate coefficients was found: Li$(1.4\pm0.4)\times10^{-2}$ s^{-1}, Na$(1.0\pm0.2)\times10^{-3}$ s^{-1}, and K$(4\pm2)\times10^{-3}$ s^{-1}. Thus the initial state formed when Li adsorbs on ice decays much more rapidly than either Na or K. The error for adsorbed K is larger, reflecting the departure of the kinetics from first order. This may reflect some time dependent evolution in this film. Despite this larger error the main result, that Li decreases much more rapidly than either Na or K, is clear.

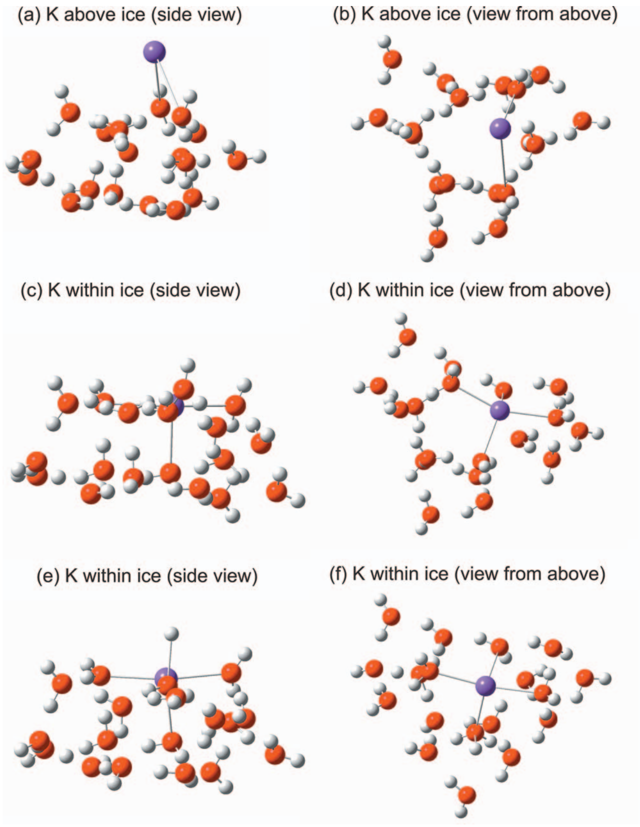
(a) K above ice (side view)
(b) K above ice (view from above)
(c) K within ice (side view)
(d) K within ice (view from above)
(e) K within ice (side view)
(f) K within ice (view from above)

FIG. 9. (Color) Calculated structures of a K atom bound to a model ice surface consisting of 18 H_2O molecules, at the B3LYP/6-311+g level of theory. The small white spheres are H atoms, the larger red spheres are O atoms, and the large purple sphere is the K atom. Panels (a) and (b) show a side- and a top-view of the K atom bound above the ice surface; panels (c) and (d) show a side- and a top-view of the K atom bound within the ice surface layer; panels (e) and (f) show a side- and a top-view of the K atom which has fully ionized leading to a stretched surface O–H bond.

In order to better understand the key observation that AM atoms bind to the ice surface with a resulting ionization potential of ~3 eV (i.e., lowered by 1.4–2.4 eV compared with the gas-phase), and also to understand why the photoelectric emission signal decreases over time, we have carried out a series of quantum chemistry calculations using the GAUSSIAN 03 suite of programs.[31] The present calculations of Li and K on ice extend our previous study[13] where we examined the binding of Na to a model ice structure which was constructed using 12 H_2O molecules to build up two stacked hexagonal rings, the top hexagon of 6 H_2O's representing the ice surface. Six additional H_2O's were added around the hexagons to simulate binding to adjacent unit cells in the ice. The calculations were performed at the B3LYP/6-311+g level of theory, which makes the geometry optimizations feasible with this number of atoms (18 O, 36 H, and 1 AM).

Figures 9 and 10 illustrate optimized structures that are relevant to understanding the experimental results for K and

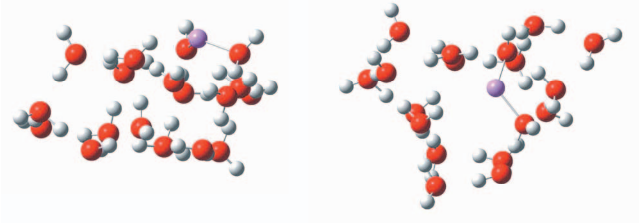

(a) Li above ice (side view)
(b) Li above ice (view from above)

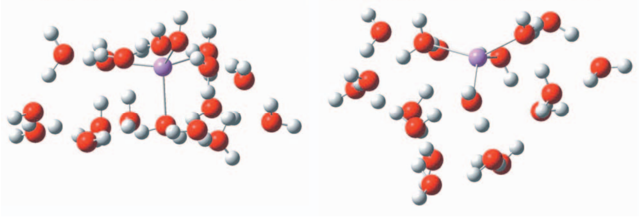

(c) Li within ice (side view)
(d) Li within ice (view from above)

FIG. 10. (Color) Calculated structures of a Li atom bound to a model ice surface consisting of 18 H_2O molecules, at the B3LYP/6-311+g level of theory. The small white spheres are H atoms, the larger red spheres are O atoms, and the purple sphere is the Li atom. Panels (a) and (b) show a side- and a top-view of the Li atom bound above the ice surface; panels (c) and (d) show a side- and a top-view of the Na atom bound within the ice surface layer.

Li, respectively. Figures 9(a) and 9(b) illustrate the optimized geometry of the $K-(H_2O)_{18}$ structure from the side and top view of the puckered hexagonal H_2O rings. This structure is the first local minimum on the potential energy surface that occurs as the K atom approaches the ice. The ice structure is least distorted in this case. The surface ring of 6 H_2O molecules has three unbound dangling H atoms (from alternate H_2O's) that point upwards from the surface. The K atom lies quite far above the surface hexagon, and is loosely bound to one of the O atoms of the H_2O's in the ring with a dangling H atom. The K–O bond length is 3.1 Å, and the Mulliken charge on the K atom is essentially zero, indicating a very weak interaction between the oxygen lone pairs and the metal. The vertical ionization energy of this structure is 4.4 eV, which is essentially the same as an isolated K atom.

If the optimization is started with the K atom in the surface hexagonal ring, the ice structure becomes distorted so that the O atoms on four H_2O's are 2.7 Å from the K, as shown in Figs. 9(c) and 9(d). The K atom is now bound more strongly, by 33 kJ mol^{-1}, and the highest occupied molecular orbital (HOMO) is more delocalized, extending to about 8 Å in diameter. This is consistent with the large photoemission cross section measured in the present study, approximately a factor of 60 larger than the PI cross section for an isolated K atom (Fig. 7). The calculated vertical ionization potential is now 3.0 eV, which is in very good accord with the measured threshold (Fig. 4).

If the optimization is started with the K atom even deeper within the ice structure, the K 4*s* electron delocalizes onto one of the H_2O molecules with a dangling surface H atom, and the O–H bond stretches significantly from 0.96 to 2.1 Å [Fig. 9(e) and 9(f)]. The Mulliken charge on the K (+0.9) indicates that the K is almost fully ionized, and the HOMO is now localized as a *p* orbital on the H atom stretched above the surface. The ionization potential of this structure is 9.3 eV, and so its formation through a thermally-activated rearrangement probably causes the photoemission signal to decay with time (Fig. 8). These results are similar to our previous experimental study and theoretical calculations on Na on ice.[16] The decay rate of K is about 4 times that of Na, consistent with the lower ionization potential of the metal. It is likely that the distended O–H bond [Fig. 9(e) and 9(f)] then breaks, and the relatively mobile H atoms recombines with another nearby H and departs from the surface as H_2, leaving KOH solvated in the ice. The driving force for the overall reaction is then the highly exothermic formation of H_2 (bond energy 432 kJ mol^{-1}). The energy of the ionized structure in Fig. (9(e) and 9(f)) is calculated to be 44 kJ mol^{-1} above that of the lowest energy structure in Fig. 9(c) and 9(d). At this level of theory an uncertainty of ±30 kJ mol^{-1} would be expected. Thus formation of the ionized structure will involve an activation energy of at least 14 kJ mol^{-1} There may also be restricted mobility of delocalized H atoms at the surface, both effects contributing to the relatively slow decay of the photoemission signal (time constant ~200 s). These results are similar to our previous experimental study and theoretical calculations of Na on ice.[13]

Figures 10(a) and 10(b) illustrate the optimized geometry of the $Li-(H_2O)_{18}$ structure from the side and top views of the H_2O rings. This structure is the first local minimum on the potential energy surface that occurs as the Li atom approaches the ice. Compared with K [see Figs. 9(a) and 10(a)], the Li atom lies much closer to the surface, binding to the O atoms of two H_2O's in the ring with a Li–O bond length of only 1.9 Å. The Mulliken charge on the Li atom is −0.1, indicating a stronger interaction between the oxygen lone pairs and the metal atom, compared with Na (Ref. 13) or K (see above). The 2*s* orbital of the Li, which is a large component of the HOMO, becomes delocalized by this interaction with the surrounding H_2O's. However, the vertical ionization energy of this structure is 3.8 eV: although this is 1.6 eV lower than the ionization potential of the isolated atom (5.4 eV), it is still significantly higher than the threshold measured in the present study (Fig. 4). If the optimization is now started with the Li atom in the surface hexagonal ring, the ice structure becomes distorted so that the O atoms on three H_2O's are 2.2 Å from the Li (the O atom on a fourth H_2O is 2.5 Å from the Li), as shown in Figs. 11(c) and 11(d). The HOMO is more delocalized, again extending to about 9 Å in diameter, in accord with the very large PI cross section (Fig. 4). The calculated vertical ionization potential is now 3.1 eV, which is in good accord with the measured threshold (Fig. 4).

In contrast with Na (Ref. 13) and K [Figs. 9(e) and 9(f)], Li does not exhibit the ionized state with a stretched surface O–H bond. The decay of the photoemission signal for Li, which is considerably faster than either Na (Ref. 13) or K (see above), must be caused by another process. The most likely candidate is the rapid diffusion of the Li atom into the bulk of the ice layer. This process will be facilitated by the smaller atomic radius [2.05 Å compared with 2.77 Å (Ref. 17)], which requires less distortion of the ice lattice [cf. Figs. 10(c) and 10(d) with Figs. 9(c) and 9(d)]. Note that if diffusion into the bulk was the primary cause of the decay of the photoemission signals from Na and K, then the Na signal would be expected to decay faster than the K signal, whereas it decays about 4 times slower.

IV. CONCLUSIONS

Photoemission from ice surfaces doped with low coverages of the alkali metals Li and K have been investigated and compared with earlier measurements for Na. A strikingly similar pattern emerges for all three AMs, given that they have significantly different PI thresholds and cross sections in the gas phase. In particular, the photoemission threshold is found to be much lower for all three AMs on ice compared with the gas phase and relatively insensitive to the identity of the AM. This is discussed in relation to the formation of a metastable delocalized but incompletely solvated electron stabilized at the water-ice–vacuum interface. The energy dependence of the photoemission spectra suggests a broad inhomogeneous site distribution for the initial state.

Calculations of the vertical ionization energies for AMs on water-ice were made. The threshold which results from the ice-AM structure minimized with the AM initially localized above the film surface yields a threshold higher than observed experimentally. If the energy minimization is made with the AM localized in the ice hexagonal ring structure, the low photoemission threshold was well reproduced for both Li and K, as it was previously for Na.[15] This suggests a kind of activated chemisorption process, with the incident AM moving through the first physisorbed minimum to localize within the ice surface. The chemisorbed state has a delocalized electron distribution, consistent with the observed large cross section.

The lifetime of the metastable initial state was determined from the decay of the photoemission signal. Li decays much faster than Na and K. For the latter pair the quantum chemical calculations suggest the formation of ionized AM and an OH^- This was not observed for Li, suggesting that the faster decay of the Li photoemission signal is caused by more rapid diffusion into the ice film.

ACKNOWLEDGMENTS

The authors are grateful to NERC for financial support of this project. T.V, was supported by a fellowship from the University Leeds.

[1] M. T. Sieger, W. C. Simpson, and T. M. Orlando, Nature (London) **394**, 554 (1998).

[2] R. E. Johnson, P. D. Cooper, T. I. Quickenden, G. A. Grieves, and T. M. Orlando, J. Chem. Phys. **123**, (2005); J. Herring-Captain, G. A. Grieves, A. Alexandrov, M. T. Sieger, H. Chen, and T. M. Orlando, Phys. Rev. B **72**, (2005).

[3] Q. B. Lu and L. Sanche, Phys. Rev. B **6315**, (2001).

[4] A. Yabushita, Y. Inoue, T. Senga, M. Kawasaki, and S. Sato, J. Phys. Chem. B **106**, 3151 (2002).

[5] P. M. Bellan, J. Geophys. Res. **113**, D16215 (2008); F. J. Lubken, M. Rapp, T. Blix, and E. Thrane, Geophys. Res. Lett. **25**, 893 (1998).

[6] C. L. Croskey, J. D. Mitchell, M. Friedrich, K. M. Torkar, U. P. Hoppe, and R. A. Goldberg, Geophys. Res. Lett. **28**, 1427 (2001).

[7] U. Bovensiepen, Prog. Surf. Sci. **78**, 87 (2005).

[8] U. Bovensiepen, C. Gahl, and M. Wolf, J. Phys. Chem. B **107**, 8706 (2003); J. Stahler, C. Gahl, U. Bovensiepen, and M. Wolf, *ibid.* **110**, 9637 (2006).

[9] J. Stahler, M. Mehlhorn, U. Bovensiepen, M. Meyer, D. O. Kusmierek, K. Morgenstern, and M. Wolf, Phys. Rev. Lett. **98**, (2007).

[10] Q. B. Lu and L. Sanche, J. Chem. Phys. **120**, 2434 (2004).

[11] Q. B. Lu and L. Sanche, J. Chem. Phys. **115**, 5711 (2001).

[12] T. Vondrak, J. M. C. Plane, and S. R. Meech, J. Phys. Chem. B **110**, 3860 (2006).

[13] T. Vondrak, J. M. C. Plane, and S. R. Meech, J. Chem. Phys. **125**, (2006).

[14] O. Havnes, J. Troim, T. Blix, W. Mortensen, L. I. Naesheim, E. Thrane, and T. Tonnesen, J. Geophys. Res., [Space Phys.] **101**, 10839 (1996).

[15] B. Baron, D. Hoover, and F. Williams, J. Chem. Phys. **68**, 1997 (1978).

[16] J. Gunster, V. Kempter, and R. Souda, J. Phys. Chem. B **109**, 17169 (2005).

[17] *CRC Handbook of Chemistry and Physics*, edited by D. R. Lide (CRC, Bocca Raton, FL, 1993).

[18] P. V. Hobbs, *Ice Physics* (Clarendon, Oxford, 1974); P. Jenniskens and D. F. Blake, Science **265**, 753 (1994); Astrophys. J. **473**, 1104 (1996); G. P. Johari, A. Hallbrucker, and E. Mayer, J. Chem. Phys. **95**, 2955 (1991).

[19] B. J. Murray and J. M. C. Plane, Phys. Chem. Chem. Phys. **7**, 3970 (2005).

[20] H. Petek, L. J. Weida, H. Nagano, and S. Ogawa, Surf. Sci. **451**, 22 (2000).

[21] K. Takeuchi, A. Suda, and S. Ushioda, Surf. Sci. **489**, 100 (2001).

[22] R. Dudde, K. H. Frank, and B. Reihl, Phys. Rev. B **41**, 4897 (1990); D. Tang, D. McIlroy, X. Shi, C. Su, and D. Heskett, Surf. Sci. **255**, L497 (1991); S. D. Parker, *ibid.* **157**, 261 (1985).

[23] R. Dudde and B. Reihl, Surf. Sci. **287–288**, 614 (1993); M. Bauer, S. Pawlik, and M. Aeschlimann, Phys. Rev. B **60**, 5016 (1999); M. Bauer, S. Pawlik, R. Burgermeister, and M. Aeschlimann, Surf. Sci. **402–404**, 62 (1998).

[24] N. Fischer, S. Schuppler, R. Fischer, T. Fauster, and W. Steinmann, Phys. Rev. B **47**, 4705 (1993).

[25] T. Vondrak and X. Y. Zhu, J. Phys. Chem. B **103**, 3449 (1999); D. Velic, A. Hotzel, M. Wolf, and G. Ertl, J. Chem. Phys. **109**, 9155 (1998).

[26] J. Zhao, N. Pontius, A. Winkelman, V. Sametoglu, A. Kubo, A. G. Borisov, D. Sanchez-Portal, V. M. Silken, E. V. Chulkov, P. M. Echenique, and H. Petek, Phys. Rev. B **78**, 085419 (2008).

[27] S. K. Jo and J. M. White, J. Chem. Phys. **94**, 5761 (1991).

[28] R. F. Reilman and S. T. Manson, Astrophys. J., Suppl. Ser. **40**, 815 (1979).

[29] H. A. Gillis and T. I. Quickenden, *Canadian Journal of Chemistry-Revue Canadienne De Chimie*, 79, 80 (2001); L. Kevan, in *Physics and Chemistry of Ice*, edited by E. Whalley, S. Jones, and L. Gold (Royal Society of Canada, Ottawa, 1973), p. 156.

[30] I. V. Hertel, C. Huglin, C. Nitsch, and C. P. Schulz, Phys. Rev. Lett. **67**, 1767 (1991).

[31] M. J. Frisch, G. W. Trucks, H. B. Schlegel *et al.*, GAUSSIAN 03, Revision B.03, Gaussian Inc., Pittsburgh PA, 2003.